Chapter 7
Magnetic Resonance Imaging (MRI) and Magnetic Resonance Spectroscopy (MRS)

Yuki Mori, Ikuhiro Kida, Haruyuki Fukuchi, Masaki Fukunaga, and Yoshichika Yoshioka

Abstract Magnetic resonance imaging (MRI) has a wide range of applications in medical diagnosis and preclinical research. MRI was invented about 40 years ago, and there are currently estimated to be over 25,000 scanners in the world. In general, contrast agents are not necessary for MRI and the soft tissue contrast of MRI is better than other imaging techniques. The important point is that MRI intensity depends on not only the concentration but also physico-chemical properties of molecules in tissues. In the first part of this chapter, several kinds of MRI techniques are described. Magnetic resonance spectroscopy (MRS) is an application of magnetic resonance. The second part of this chapter is concerned with MRS. This technique provides information in metabolism non-invasively, and obtains spectra from a region of interest two- and three-dimensionally. Some physiological parameters, such as pH and temperature, can be estimated by the spectra. Applications of MRI and MRS are very broad, since many factors affect MRI signals. Functional MRI (fMRI) is an important application used widely in the neurosciences, human sciences, and economics, as well as in medical sciences. The major restriction of MRI is its long scan time. An accelerated technique is described in the last part of the chapter.

Keywords Magnetic resonance imaging • Magnetic resonance spectroscopy • fMRI • Cell tracking • Compressed sensing

7.1 Introduction of Magnetic Resonance

The magnetic resonance method to measure the nuclear magnetic moment was discovered in the laboratory of Rabi (Rabi et al. 1938). This discovery was made in the context of molecular beam experiments in which individual, isolated atoms or

Y. Mori • I. Kida • H. Fukuchi • M. Fukunaga • Y. Yoshioka (✉)
Immunology Frontier Research Center, Osaka University, Suita, Osaka, Japan

Center for Information and Neural Networks, National Institute of Information and Communications Technology, Suita, Osaka, Japan
e-mail: yoshioka@fbs.osaka-u.ac.jp

M. Kasaki et al. (eds.), *Cognitive Neuroscience Robotics B*,
DOI 10.1007/978-4-431-54598-9_7

molecules were the objects of investigation. The nuclear magnetic resonance (NMR) in a bulk sample was first reported independently by two groups (Purcell et al. 1946; Bloch et al. 1946). The chemical shift, which measures resonance frequency variations according to the nuclear chemical environment, was subsequently discovered (Arnold et al. 1951), and the NMR method came to be used for chemical structure analysis and research into physical properties. In 1971, extensions of longitudinal and transverse relaxation times, which are physical properties of the NMR phenomenon, were discovered in pathological tissues and compared with normal tissues (Damadian 1971). This suggested the possibility of applying NMR for pathological analysis. In 1973, the first MR image was reported (Lauterbur 1973). This was the starting point of magnetic resonance imaging (MRI) techniques. During the 1970s and 1980s, the development of MRI for clinical use in medical practice was pushed forward extensively by universities and companies. As a result, image quality improved dramatically and clinical scanners proliferated worldwide. Overall, this rapidly growing field encompasses an array of disciplines, and many new developments continue to emerge. The introduction of MRI and magnetic resonance spectroscopy (MRS) to brain research has dramatically altered our understanding of the brain in recent decades. Today, MRI and MRS techniques have become indispensable tools for both the clinical diagnosis of brain disorders and basic neuroscience research. Recent developments in MRI and MRS (i.e., ultra-high field MRI, multi-channel RF systems, etc.) allow measuring high resolution in vivo human brain images on the order of several hundred microns; however, such high resolution MRI requires unreasonably long scanning times for whole brain acquisition. Over the last decade, efficient data sampling schemes and high precision data reconstruction methods (i.e., sparse sampling or compressed sensing) were introduced in MRI, which brought about a dramatic reduction in acquisition times.

In this chapter, we discuss the basics of MRI and MRS, especially for brain research, and compressed sensing in MRI.

7.2 Anatomical Information Obtained by MRI

The magnetic resonance imaging (MRI) method is used to depict the anatomical structure of the brain non-invasively. Various brain structures, such as the corpus callosum, pituitary, medulla, cerebellum, caudate nucleus, putamen, and so on, are easily identified on the magnetic resonance images in Fig. 7.1. The corpus callosum displays low signal intensity, and the cerebrospinal fluid around the medulla and cerebellum displays high intensity.

MRI signal intensity is determined by the concentration and physico-chemical properties of water in the region of interest. For example, the signal intensity of the cerebrospinal fluid is higher than that of brain tissues because the water concentration of the former is higher than that of the latter. The concentration and physico-chemical properties of water depend not only on its structure but also on many other factors, such as inflammation, edema, lipid content, susceptibility, and so on. For this reason, MRI is sensitive to pathological changes in disease. MRI has become a

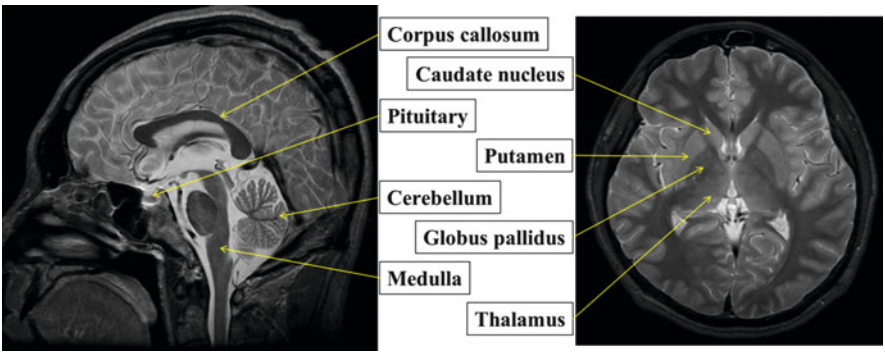

Fig. 7.1 MRI anatomy of the normal adult human head

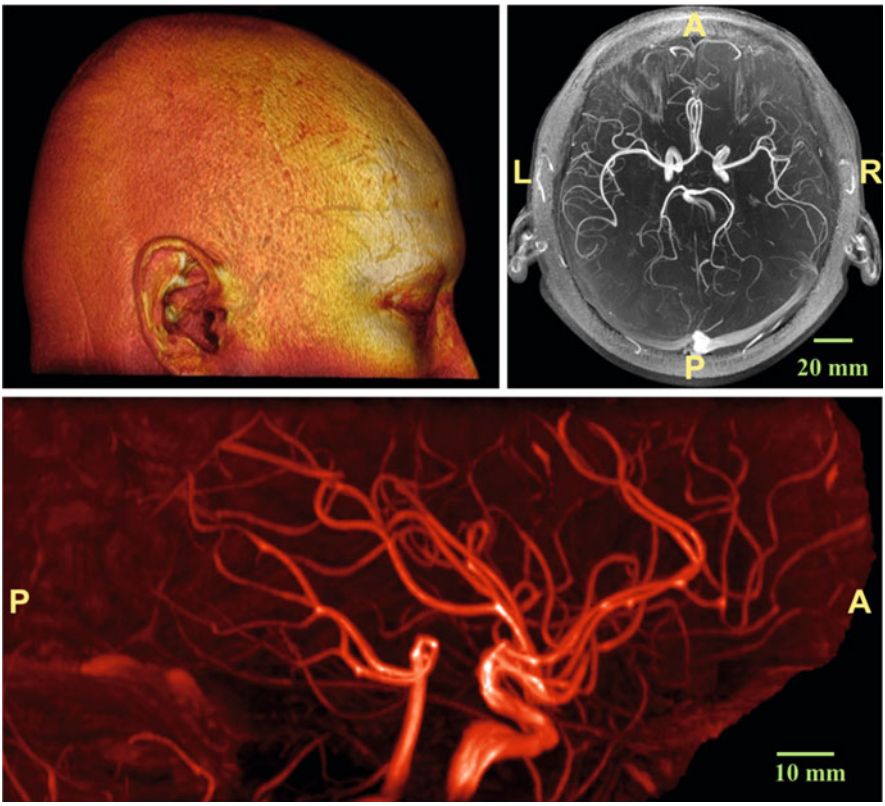

Fig. 7.2 Blood vessels in the healthy human brain. *Upper right*: top-down view of brain blood vessels. *Lower*: side view of brain blood vessels. Nearly all vessels visualized in this case are arteries. Veins can be visualized by other MRI techniques (MR venography or susceptibility weighted image (SWI))

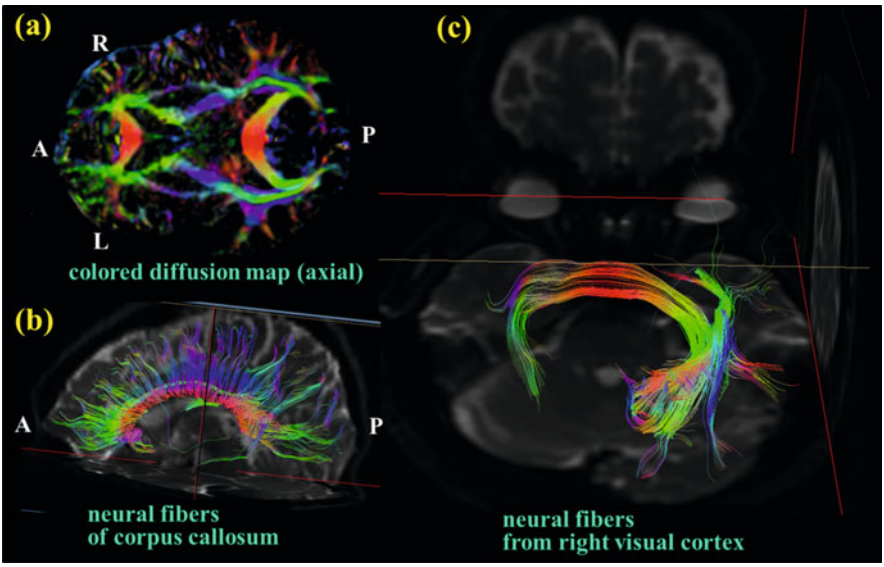

Fig. 7.3 Diffusion anisotropy map and neural fiber tracking of the human brain (anatomical connectome). Tracking was performed using information on the anisotropic diffusivity of water molecules in neural fibers

necessary diagnostic method and has been used in many clinical and pre-clinical studies. High resolution sub-millimeter images are obtained with modern 3 T MRI scanners.

MRI signal intensity also depends on the flow of water, typically the flow of blood in the body. Flowing blood can be visualized by MRI, as shown in Fig. 7.2 (Haacke et al. 1999). Blood flows through blood vessels. An important point is that blood vessels can be visualized using MRI without contrast reagents. Blood vessel imaging is called "magnetic resonance angiography" (MRA). MRA has been employed in clinical and pre-clinical studies.

Diffusion weighted imaging (DWI) is a type of MRI that provides information on the diffusivity of water molecules (Brownian motion, not flow) from MRI signal intensity (Le Bihan et al. 1986). Since the diffusivity of water molecules changes markedly immediately after the onset of a disease, e.g., cerebral infarction (stroke), DWI provides an important way to assess acute stroke. The major cause of the change in the DWI signal during ischemia is cell swelling, i.e. the movement of water molecules from the interstitial space (high diffusivity) into cells (low diffusivity) (Moseley et al. 1990). Since water diffusion also significantly decreases in malignant tissues, DWI is considered to have the potential to detect malignant cancers.

Information on the three-dimensional diffusivity of water molecules can be added to DWI data (Basser et al. 1994). Since water molecule diffusion is anisotropic in muscle and neural fibers, the running directions of these fibers can be visualized by the information from anisotropy (Fig. 7.3a). The colors indicate the

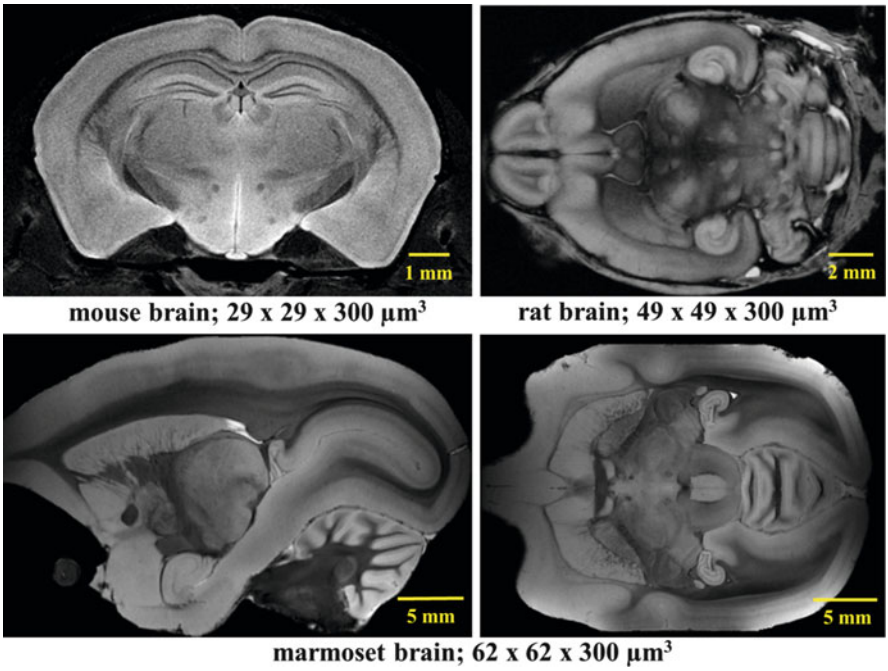

Fig. 7.4 High resolution brain images of a mouse, rat, and marmoset. These fine images were obtained non-destructively using an 11.7 T MRI scanner

directions of neural fibers as follows: red: left-right, green: anterior-posterior, and blue: top-down. These fibers can also be tracked by tracing the most diffusive directions in the pixels (Mori and Barker 1999; Mori 2007). Figure 7.3b, c show the tracking of neural fibers in the human brain. The meaning of the colors is the same as in Fig. 7.3a.

One of the major limitations of the past MRI techniques was their spatial and temporal resolution. The resolution of MRI is determined by the signal to noise ratio (SNR), as in other imaging methods. Recently, ultra-high magnetic field MRI scanners (higher than 7 T) have been introduced, and they provide fine MR images at cellular resolution with animal scanners and at several hundred micrometers with human scanners. Ultra-high field scanners produce new tissue contrasts and fine vascular images. Tissues and organs of laboratory animals are sometimes fixed and stained in order to increase resolution and contrast (the scan time can be increased as well). Figure 7.4 shows MRI images of ex vivo animal brains provided by an 11.7 T MRI scanner.

These fine anatomical images are usable for histological assessments. In addition, since contrast agents of MRI are applicable in both in vivo and ex vivo studies, precise histological information can be obtained (Zhang et al. 2010). Magnetic resonance histology (or MRI histology) is one of the new applications of MRI for the study of tissues and organs.

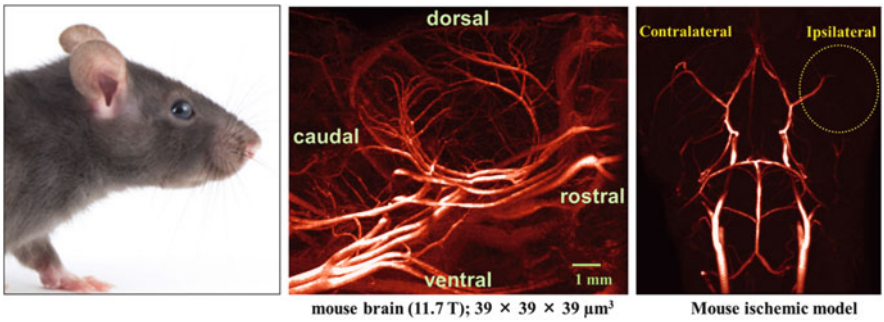

Fig. 7.5 Visualization of blood vessels in a living mouse brain. *Center image*: side view of brain blood vessels (normal mouse). *Right image*: top-down view of brain blood vessels (the right MCA was occluded)

MR angiography (MRA) has been used in mice, as is shown in Fig. 7.5. Highly sensitive MRI scanners and optimized probe coils make it possible to visualize blood vessel trees in detail, even in the small mouse brain. They can be used to assist in the diagnosis of neovascularization and degenerative vascular changes following traumatic brain injury, ischemia, dementia, and so on.

Recent studies with a high-field animal MRI scanner have revealed that with specific contrast agents, the cells of a living mouse can be labeled and traced at the single cell level, and the distribution of labeled cells can be visualized (Mori et al. 2011; Mori and Yoshioka 2012).

Though it is a longstanding assumption that the central nervous system (CNS) is an "immune privileged site", some reports have demonstrated that immune cells in the CNS play an important role in neuroinflammatory diseases, such as multiple sclerosis and ischemic injury. However, the dynamic crosstalk between the CNS and immune cells has not been characterized by non-invasive imaging techniques. The non-invasive visualization of immune cell dynamics and immunological responses in vivo before/after neuroinflammatory conditions may lead to a greater understanding of the mechanistic underpinnings of CNS diseases and their repair. As a first step, it is important to elucidate immune cell dynamics in the CNS. MRI at 11.7 T provides a way to visualize immune cell dynamics and immune responses non-invasively. Figure 7.6 shows the accumulation of immune cells (black dots) in and around an inflammatory brain lesion (hyperintensity region). These images are obtained before and after brain injury. Labeled immune cells are detected in and around the injured region. Each small dark spot corresponds to a single cell.

In conclusion, the MRI techniques that are recently developed can adequately provide precise morphological information at the cellular and tissue levels, and such information is useful for pre-clinical studies. Many developments of MRI aim at overcoming its limitations in resolution, contrast and specificity, and MRI image quality and information precision are increasing day by day.

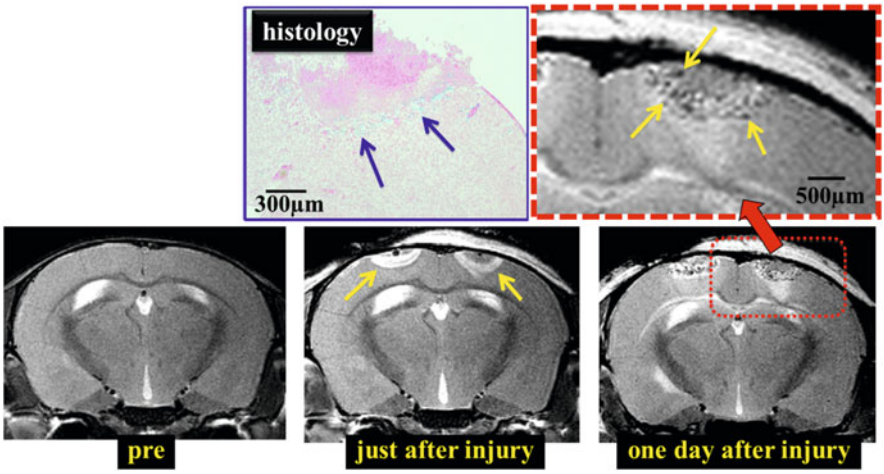

Fig. 7.6 MRI image 1 day after injury shows the accumulation of labeled immune cells in and around the injured region

7.3 Magnetic Resonance Spectroscopy

7.3.1 Introduction

Magnetic resonance imaging (MRI) and spectroscopy (MRS) are both based on the properties of spins in atomic nuclei. MRS is an analytical method used for the identification of chemical compounds and molecular interactions in physics and chemistry. MRS is also used in biological and biochemical studies to quantify and characterize biomolecules, and it can even be used in vivo. Proton MRS (^{1}H) is often used in biological studies because of the high natural abundance of hydrogen atoms in biological systems and the high sensitivity of the proton signal in this method (Table 7.1). While information provided by MRI is based on the water content, molecular information gathered by MRS is based on the chemical environment of nuclei.

MRS has some advantages over MRI. MRS can directly and specifically measure metabolite and neurotransmitter concentrations in the cells of brain and muscle tissues. Spectra detected by MRS have several peaks whose positions depend on the electron environment of chemical functional groups in molecules. This dependency is called a "chemical shift." MRS provides metabolic and physiological information, such as cell density, viability, energy metabolism, temperature, and pH, and such information can be helpful in disease diagnosis. On the other hand, MRI has some advantages over MRS. MRI is generally used to detect proton nuclear signals and the water content. When water is abundant in biological systems, MRI has high sensitivity and high spatial and temporal resolution. ^{1}H MRS detects low concentrations of metabolites, ranging from 1 to 15 mM; this low as compared with water (~40 M) in biological systems. Since MRS has low sensitivity, it can only yield a

Table 7.1 MRS properties of nuclei

Isotope	Spin	Natural abundance (%)	Gyromagnetic ratio (10^7 rad/T/s)	NMR frequency at 2.35 T	Relative sensitivity
^{1}H	1/2	99.985	26.752	100.000	1.00
^{13}C	1/2	1.108	6.728	25.145	1.76×10^{-4}
^{17}O	5/2	0.037	−3.628	13.562	1.08×10^{-5}
^{19}F	1/2	100	25.181	94.094	0.834
^{23}Na	3/2	100	7.080	26.466	9.27×10^{-2}
^{31}P	1/2	100	10.841	40.481	6.65×10^{-2}

sufficient signal from a single voxel beyond several centimeters if used for several minutes; detection of a signal from multiple voxels beyond several centimeters takes several tens of minutes. For example, MRI could yield an anatomical image of a whole brain (roughly 20 cm in diameter, with a voxel size of several hundred micrometers) in several minutes. However, it can provide a highly temporal image of a whole brain (with a voxel size of several millimeters) in several hundredths of a millisecond. ^{1}H and ^{31}P MRS are used in clinical applications to measure metabolites *in vivo*.

Metabolite and neurotransmitter signals on MRS appear as peaks at different positions depending on the chemical shift. Since all the metabolic intermediate compounds contain hydrogen, carbon, and phosphorus nuclei, MRS in principle can detect all the metabolic compounds at different positions on the spectrum and measure their concentrations as signal peak areas. However, it is difficult to detect most metabolic intermediates if their concentrations are too low at a specific chemical shift or if there is overlap between peaks of different metabolites. The use of MRS is mostly limited to the brain, where there are few motion artifacts and low amounts of lipids.

7.3.2 Proton MRS

Proton MRS can simultaneously display the resonance peaks of metabolites and neurotransmitters in biological systems, such as the brain (Fig. 7.7). Since metabolites and neurotransmitters contain hydrogen nuclei, ^{1}H MRS is a powerful tool for detecting a large number of metabolites in vivo (Table 7.2). ^{1}H MRS of the brain detects a spectrum of metabolites, including *N*-acetyl aspartate, creatine and phosphocreatine, choline, myo-inositol, glutamate, and glutamine (Ross and Blüml 2001).

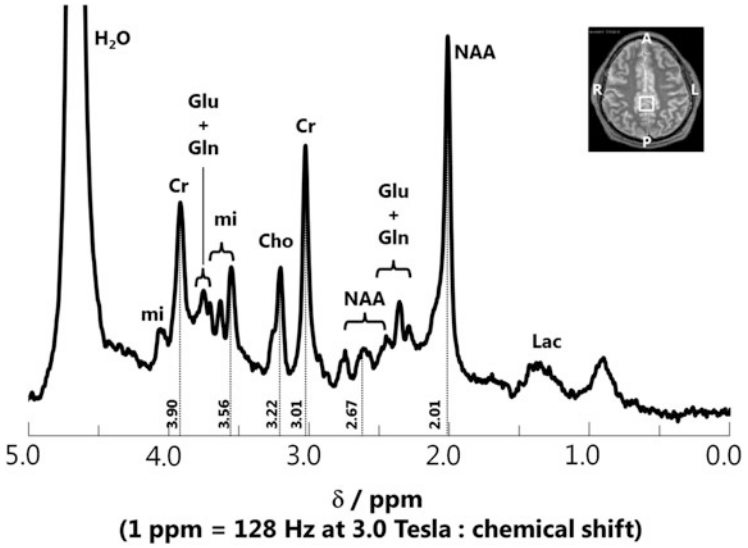

Fig. 7.7 Proton MR spectrum obtained from human brain at 3.0 T (TR/TE = 3000 ms/30 ms; 2 cm × 2 cm × 2 cm) with partial water suppression. The voxel positions are indicated in the MR image. *Cr* total creatine, *mi* myo-inositol, *Cho* choline, *Glu* glutamate, *Gln* Glutamine, *NAA* N-acetyl aspartate, *Lac* lactate

Table 7.2 Proton MRS – observed metabolites

Metabolite	Main resonance (ppm)	Concentration in human brain (mM)	Significance
Lactate	1.33	0.2–1.0	Anaerobic glycolysis
NAA	2.01 and 2.49 and 2.67	8–12	Neuronal and axonal density and viability
Glutamate	2.0–2.5	6–12	Neurotransmitter and TCA cycle
Glutamine	2.0–2.5	1.5–6.0	Neurotransmitter and TCA cycle
GABA	2.0–2.5	1.0–2.0	Neurotransmitter and TCA cycle
Total Cr	3.01 and 3.90	4.5–10	Energy metabolism
Cho	3.22	0.5–2.5	Membrane metabolism and cell proliferation
Myo-inositol	3.56	4.0–9.0	Glial marker

Hetherington et al. (1994), Pan et al. (1998), Pouwels and Frahm (1998), and Wang and Li (1998)

7.3.2.1 *N*-Acetyl Aspartate

As Fig. 7.7 illustrates, *N*-acetyl aspartate (NAA) generates the most prominent peak at 2.01 ppm from a CH_3 group and smaller peaks at 2.49 and 2.67 ppm from a CH_2

group. NAA is synthesized from L-aspartate and acetyl-Co-A by the enzyme L-aspartate-N-acetyl-transferase. This enzyme, which is only detectable in the nervous system, is found in the mitochondria (Goldstein 1969) and cytoplasm of neurons. Since NAA is specifically and stably localized in neurons and axons of the adult brain, NAA is considered to be a marker of neuronal density and viability (Moffett et al. 2007; Signoretti et al. 2001). NAA is also found in the progenitor cells of oligodendrocytes and astrocytes (Urenjak et al. 1992) and increases in concentration during the maturation of the cerebellum, thalamus, and grey matter. Care is thus needed when NAA is used as a marker for neurons and axons during maturation. NAA is also used as a reference for other metabolite concentrations. Since NAA concentrations vary in different regions of the brain (Pouwels and Frahm 1998; Wang and Li 1998), care is needed when using NAA as a reference. A decrease in NAA concentration reflects degeneration of neurons and axons, and may indicate mitochondrial dysfunction. Mitochondrial dysfunction may occur in neurological disorders, such as epilepsy, hypoxia and multiple sclerosis (MS) (Signoretti et al. 2001). The physiological functions of NAA have not been fully elucidated, even though the localization of NAA to neurons is well known. Suggested physiological functions include (i) osmoregulation, i.e., removing water from neurons and counter anions in neurons (Taylor et al. 1995), and (ii) serving as a precursor for the production of N-acetyl aspartic glutamate (Moffett et al. 2007).

7.3.2.2 Creatine and Phosphocreatine

The primary peaks at 3.01 ppm from a CH_3 group and at 3.9 ppm from a CH_2 group represent the combination of two compounds: phosphocreatine (PCr) and creatine (Cr); the combination is referred to as 'total Cr.' Since both compounds relate to ATP reserves, each of these peaks is regarded as a marker of energy metabolism (Ross and Blüml 1996). Since total Cr is relatively stable in the human brain at 6–8 mM (regardless of age), total Cr is often used as an internal reference for the relative concentrations of other brain metabolites. The ratio of metabolites to total Cr can be calculated (e.g., NAA/Cr) (Li et al. 2003). However, since the total Cr concentration varies with brain region (higher in the gray matter than in the white matter) (Pouwels and Frahm 1998), care should be taken when using total Cr concentrations as a reference. In addition, total Cr increases during trauma and decreases in hypoxia, stroke, and tumors.

7.3.2.3 Choline

The peak at 3.22 ppm represents the combination of choline and choline-containing compounds, such as phosphocholine and glycerophosphocholine. Choline and its metabolites have three main physiological purposes: providing structural integrity, signaling in cell membranes, and facilitating cholinergic neurotransmission. Choline is a precursor of the neurotransmitter acetylcholine, which has many functions,

including memory and muscle control. Choline is also a precursor of phosphatidylcholine, a major constituent of cell membranes (myelin sheaths in particular). Phospholipids are released during myelin breakdown, leading to an increase in choline concentration. Choline is thus a marker of cell membrane turnover. The concentration of choline is higher in the white matter than in the grey matter (Pouwels and Frahm 1998), and the concentration of choline in glial cells can be twice as high as that in neurons (Gill et al. 1989). The highest levels of choline are present at birth, and decrease with age. In adults, an increase in choline is associated with Alzheimer's disease, chronic hypoxia, and epilepsy.

7.3.2.4 Myo-inositol

The main peak at 3.56 ppm and smaller peaks at 3.61 ppm and 4.05 ppm from a CH group include 80 % myo-inositol and 10–20 % inositol-monophosphate. Myo-inositol occurs primarily in glial cells and is incapable of crossing the blood-brain barrier; thus, this compound is a specific glial marker (Brand et al. 1993). Myo-inositol is abundant in the newborn brain and decreases during brain development. In the adult human brain, an increase in myo-inositol is regarded to indicate glial proliferation or an increase in glial cell size, both of which occur during inflammation (Soares and Law 2009). Myo-inositol also increases in Alzheimer's disease and diabetes mellitus, and decreases in stroke, tumor, and hypoxia encephalopathy.

7.3.2.5 Glutamate, Glutamine, and γ-Aminobutyric Acid (GABA)

The peaks between 2.0 and 2.5 ppm are signals from the combination of protons in glutamate, glutamine, and GABA (β- and γ-CH_2 for glutamate and glutamine; β- and α-CH_2 for GABA). The peaks between 3.6 and 3.8 ppm are signals from the combination of protons (α-CH) in glutamate and glutamine. The peak at 3.00 ppm is GABA from γ-CH_2, but it is usually undetected because of the overlap with a large total Cr peak. Measurement at a higher magnetic field strength can improve the quantification of these compounds.

Glutamate is the most abundant excitatory neurotransmitter in the brain. It has been shown to increase in patients with multiple sclerosis (in both demyelinating lesions and apparently normal white matter) (Srinivasan et al. 2005). Glutamine is an intermediate molecule produced from glutamate in astrocytes; thus, this molecule serves as an astrocyte marker. Glutamine may increase in hepatic encephalopathy, hypoxic-ischemic events, and hyperosmolar states, and decrease in Alzheimer's disease and hyponatremia. GABA is the major inhibitory neurotransmitter in the brain. GABA is produced by the glutamate decarboxylase from glutamate in the mitochondria. GABA is associated with several neurological and psychiatric disorders, including depression and epilepsy. The glutamate-glutamine (and/or GABA) cycle exists in pre-synaptic and astroglial cells. Glutamate

(or GABA) is released from the pre-synaptic into the cleft. After interaction with post-synaptic cells, glutamate is taken by the Na/K pump into the astroglia, where it is then converted to glutamine by glutamine synthetase. Glutamine is transported back to neurons, where it is converted to glutamate. This glutamate-glutamine cycle is similar to the GABA-glutamine cycle between neurons and astroglia (Magistretti and Pellerin 1999).

7.3.2.6 Lactate

Lactate appears at 1.33 ppm but is usually not observed in normal brain spectra. Lactate is associated with glucose metabolism and measured immediately after stimulus onset in the visual cortex (Prichard et al. 1991; Frahm et al. 1996). Lactate is mainly detected in patients with stroke, tumor, hypoxia, and anoxia.

7.3.3 Phosphorous MRS

Phosphorous (^{31}P) MRS is used to measure high energy phosphorus compounds, such as adenosine triphosphate (ATP), phosphocreatine (PCr), and inorganic phosphate (P_i). These compounds relate to energy metabolism in the brain, muscle, liver, and heart. ^{31}P MRS provides high quality spectra in several minutes because of its relatively high sensitivity (approximately 7 % of ^{1}H MRS) and high natural abundance of phosphorus in the body. Since ^{31}P MRS has a relatively large chemical shift difference (e.g., 30 ppm compared to 10 ppm in ^{1}H MRS), its spectral resolution is high even in the low magnetic fields used in clinical applications (Fig. 7.8).

The peaks of the main metabolites are measured by ^{31}P MRS as follows: phosphomonoesters (PME) (6.5 ppm), P_i (4.9 ppm), phosphodiesters (PDE) (2.6 ppm), PCr (0 ppm); ATP has three peaks: −2.5 (γ), −7.5 (α), and −16.3 (β) ppm. The peaks of adenosine diphosphate (ADP) at −7.1 (α) and −3.1 (β) ppm overlap with the ATP peaks. Nicotinamide adenine dinucleotide (NADH/NAD) has an additional peak at −8.3 ppm. Cellular energy metabolism is represented by ATP, PCr, and P_i, with PCr serving as a high energy phosphate storage compound in brain and muscle tissues. The PDE and PME compounds are related to membrane phospholipids. An increase in PME has been associated with rapid tissue growth or rapid membrane synthesis. PME has also been found to increase in the infant brain and in tumors. PCr resonance is conventionally used as an internal chemical shift reference between ATP and P_i. In addition, since the chemical shift of the peak in P_i is pH dependent, the chemical shift between P_i and α-ATP or PCr is commonly used to estimate intracellular acidity (pH) *in vivo*.

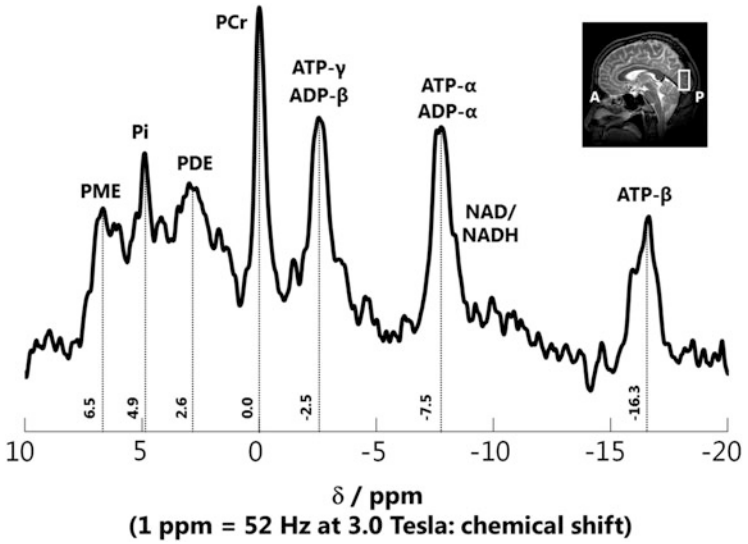

Fig. 7.8 Phosphorous MR spectrum obtained from human brain at 3.0 T (TR/TE = 1000 ms/2.5 ms; 4 cm × 4 cm × 2 cm). The voxel positions are indicated in the MR image. *PME* phosphomonoesters, P_i inorganic phosphate, *PDE* phosphodiester, *PCr* phosphocreatine, *ATP* adenosine triphosphate, *ADP* adenosine diphosphate, and *NAD/NADH* nicotinamide adenine dinucleotide

7.3.4 Carbon MRS

If a biological system has a low natural abundance of ^{13}C and the sensitivity of ^{13}C detection (1.1 %; on the order of 10^{-4}) is low, measurements can take several tens of minutes. For this reason, clinical application of ^{13}C MRS is difficult. However, since the chemical shift difference is large (300 ppm, with specific peaks), the spectral resolution of ^{13}C MRS is high and chemical shifts are easily assigned. Furthermore, in contrast to ^{31}P MRS, ^{13}C MRS can detect a large number of metabolites. Because of its low sensitivity, ^{13}C MRS requires administered isotopes, such as ^{13}C-glucose and ^{13}C-acetate. ^{13}C-glucose enters the normal metabolic pathway of ^{12}C-glucose and has no toxic effects, allowing for the assessment of metabolic changes. ^{13}C-glucose can be used to determine the rate of the tricarboxylic acid cycle in relation to the cerebral metabolic rates of oxygen and glucose.

7.3.5 Summary

In the last few years, human MR systems with magnetic field strengths higher than 3.0 T have been developed. The development of coils and optimization of the RF pulse have led to greater sensitivity, faster acquisition, and higher spatial resolution

for the clinical use of MR systems. Spectral resolution has been improved by stronger magnetic fields (better spectral separation between peaks). Concerns have been raised with regard to increased magnetic fields: inhomogeneity, structure-activity relationship limitations, and the problem of shimming. Practical and precise localization techniques are crucial for achieving the best field homogeneity and for effective water suppression. Despite these disadvantages, MRS is a powerful and promising tool for providing metabolic and viability data of biological systems. MRS uses the same system as MRI and provides structural and anatomical information.

7.4 Functional Magnetic Resonance Imaging (fMRI)

7.4.1 BOLD fMRI

Magnetic resonance imaging (MRI) methods can clearly depict the morphological information both in clinical and in pre-clinical studies (Fig. 7.1). MRI is a useful and innovative imaging modality for non-invasive and simultaneous imaging of both morphological changes and cellular migration, even if the regions of interest are located in deep tissues and organs.

Functional magnetic resonance imaging (fMRI) of the brain is a non-invasive technique for measuring brain activity using MRI signal changes associated with brain neuronal activities. An example of fMRI during visual stimulation is shown in Fig. 7.9.

The most widely used method is based on the mechanism of BOLD (blood oxygenation level-dependent) contrast. It works by detecting changes in the blood oxygenation level that occur in response to local neural activities (Ogawa et al. 1990; Ogawa and Sung 2007). Since the electronic spin state of heme iron in deoxyhemoglobin is 2 (high spin state), deoxyhemoglobin is paramagnetic (Pauling and Coryell 1936) and has an effect on the MRI signal. Deoxyhemoglobin is a naturally occurring contrast agent for MRI. Oxyhemoglobin, on the other hand, has no effect on MRI parameters because the spin of heme iron is zero (low spin state). Therefore, the MRI signal depends on the blood oxygenation level. This magnetic property of blood was reported by Thulborn et al. in 1982 in an in vitro blood experiment. The blood oxygenation level changes during brain activation due to an increase in oxygen usage and a change in blood flow. The regional cerebral blood flow is changed by neurovascular coupling and is affected by the metabolites produced by neurons and glial cells during activation. In general, since the oxygen supply by blood flow overcompensates the oxygen demand of activated neurons, the blood oxygenation level increases during brain activation, and the MRI signal intensity increases. BOLD-fMRI was originally designed to detect activated brain areas using the rest-task protocol shown in Fig. 7.9b. fMRI can be used to produce activation maps that show which parts of the brain are involved in a particular

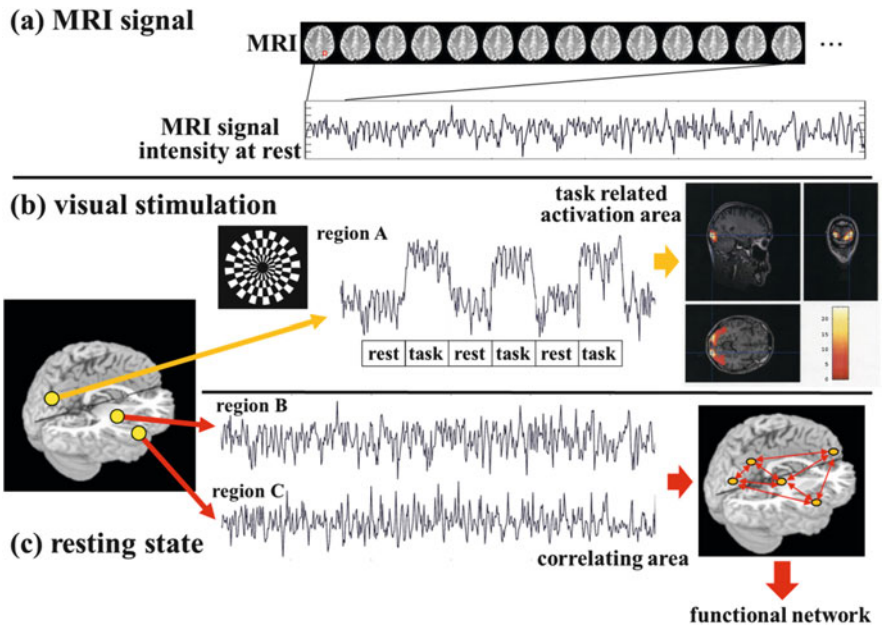

Fig. 7.9 (**a**) MRI and MRI signal fluctuation with time. This fluctuation contains physiological modulations as well as artificial noise. (**b**) Task-related fMRI. (**c**) Resting state fMRI. Correlated regions are picked up

mental process. fMRI is an important application of MRI and used widely in neurosciences, human sciences, and economics, as well as in medical sciences (Greene and Haidt 2002; Bandettini 2012).

The main disadvantage of BOLD-fMRI over magnetoencephalography (MEG) and electroencephalography (EEG) is slow response time, and it is common to all measurements based on vascular changes. Vascular changes (hemodynamic responses) appear a few seconds after the start of neural activation. If events occur in short time scales relative to the fMRI response time, it is not easy to resolve individual events by fMRI.

The development of various non-invasive fMRI measurements other than BOLD-fMRI has been challenged. Cerebral blood flow (CBF) and cerebral blood volume (CBV) measurements, both of which are based on the vascular response like as BOLD-fMRI, have good specificity and sensitivity for activated blood vessels (Ogawa and Sung 2007). It has been shown that diffusion MRI signals respond to neuronal activation and their signal change has good spatial resolution (Le Bihan et al. 2006). This diffusion weighted MRI appears to reflect a change in the apparent diffusion constant (ADC) of water in the brain. The response could be explained by the swelling of neurons during neuronal activation. Direct detection of electromagnetic events caused by brain activity has also been tried using MRI. However, the direct in vivo detection of electromagnetic events is still challenging.

7.4.2 New Wave of fMRI – Resting State fMRI, Functional Connectivity (Connectome)

Figure 7.9b shows a typical block paradigm of event-related fMRI and Fig. 7.9c a resting-state fMRI experiment. Resting-state fMRI is a relatively new method to study spontaneous fluctuations in brain activity during the resting state (the subject is not performing an explicit task). A long MRI time series data analysis shows that the spontaneous low-frequency (<0.1 Hz) BOLD signal fluctuations under resting conditions often have strong correlations even in distant brain regions (Biswal et al. 1995). The distributed patterns of resting-state fMRI correlations are relatively consistent over several brain states; these patterns are so-called resting state networks (Fox and Raichle 2007). The biological significance of these spontaneous, correlated activities in the resting brain remains unclear; however, the study of resting state networks has already been shown to have potential clinical value, providing rich and sensitive markers of disease (Fox and Greicius 2010).

7.5 Introduction to Compressed Sensing (Faster Imaging Technology)

7.5.1 Introduction

Magnetic Resonance (MR) has many applications in biological science and industry. MR Imaging has been widely used in medical diagnosis because of its non-invasive manner and exquisite detail in images of soft tissues. The major restriction to the use of MRI is its long scan time.

The physical processes of excitation and reception of MR signals are inherently quite slow. To measure a MR signal takes milliseconds per pulse. The hardware of MRI has been developed and improved dramatically, but hardware development cannot shorten the physical processes required to acquire MR signals. MRI raw data are collected first in the frequency domain (called the 'k-space'). The data acquisition speed (k-space traversal speed), which depends on the gradient switching speed, is limited because of the current produced by the high power and high speed switching of gradient coils stimulate peripheral nerves. The gradient switching speed is restricted so as not to go over the limits of peripheral nerve stimulation. Further acceleration of the MR system requires alternative techniques. Many researchers are seeking for a new method of acceleration.

The reduction of scan time is an ongoing challenge. Many methods, such as parallel imaging and other undersampling strategies, have been invented to enable imaging of fast biological processes. Fundamentally, these methods utilize the redundancy of data (e.g., multiple receiver coils are designed to generate redundant data per acquisition). These techniques are mostly governed by the Nyquist sampling rate, and hence they cannot yield acceleration greater than the Nyquist limit

due to the resulting aliasing artifacts. The Nyquist limit is the minimum sampling rate required to avoid aliasing; the sampling rate for any signal must be at twice the highest frequency contained within the signal.

On the other hand, compressed sensing (CS) (also known as compressive sampling) can recover the signal below the Nyquist limit. CS is a fundamentally new approach to data acquisition. CS can reconstruct sparse signals and images from what was previously believed to be incomplete information. Hence, CS has gained attention in signal processing, statistics, and computer science.

7.5.2 Compressed Sensing

Every day, we use data compression to process images and audio signals. Conventional data compression techniques take the full data set at the beginning. For example, after one takes a picture (full information) and acquires an entire image, compression tools encode a few significant data (most of the information is thrown away) and store it. One can decode and reconstruct the original entire image from the stored data. As this example shows, there is unnecessary data in original images. If there is a wise way to measure compressed data directly from the real world, only a small number of measurements are needed. This is a valuable line of approach for MRI because MRI measurements are expensive and slow. CS opens the door to this approach. The theory of compressed sensing was put forward by Candes et al. and Donoho (Candès et al. 2006; Donoho 2006). They pointed out that signals can be reconstructed from a very limited number of samples, provided that the measurements satisfy an incoherence property.

Since the CS acquisition process corresponds to the measurement of compressed data of images, CS requires images to be compressible on some basis. The image property that lies behind compressibility is sparsity: under transformation, many of the data values in the transform domain can be set to zero and the image can be reconstructed from the rest of the data without an appreciable effect. In other words, if a significant majority of the data or vectors have coefficients equal to zero and a few coefficients of it contain all the information, the data or vector is sparse.

The CS approach requires the following:

1. Random sampling (incoherence of undersampling artifacts)
2. Sparse signals in some basis (transform sparsity)
3. Non-linear reconstruction

Random sampling ensures the incoherence of undersampling artifacts; this means that aliasing is produced by sampling below the Nyquist limit. Sparsity of data defines the important coefficients that are used for reconstruction of the original signal. How many coefficients are required for reconstruction is decided by a threshold. The measured data used in the CS acquisition process is already compressed, and hence reconstruction of the original data functions as a decoding process.

7.5.3 Applying Compressed Sensing to MRI

The application of CS to MRI potentially provides significant scan time reductions, leading to benefits for patients and health care economics. It is also beneficial for the measurements of high speed biological processes, such as cardiac and rapid angiography.

The first point to be discussed is under what conditions CS can be applied to MRI. The application of CS in MRI has the following restrictions:

1. MRI data should be collected by random sampling
2. MRI images should be sparse (or transform domain)
3. Images should be reconstructed by nonlinear methods

The MR system acquires MR signals as encoded samples, and this allows CS to be successfully applied to MRI. MRI measures not direct pixel samples but rather the Fourier coefficients of an image. A common approach is to use undersampling to reduce the number of readout lines in the grid of the k-space (this undersampling pattern corresponds to sparse sampling in phase direction). Other sampling patterns, e.g., radial sampling, are also available.

Most MR images are compressible by sparse coding in an appropriate transform domain (e.g., by wavelet transform). For example, the images of MR angiography—consisting of contrast enhanced blood vessels with a black background—are already sparse in the pixel representation and also sparse in the finite differences domain. Other examples are cardiac cine images. They are sparse in the spatio-temporal Fourier domain. More complex images, such as brain images, can be sparsified in the wavelet transform domain.

It is important for the reconstruction process to impose a nonlinear regularization, such as the L_1 norm. The non-linear reconstruction process has consistency with acquired data, as a subset of the k-space data.

This raises the questions as to how to decide on the minimum number of measurements (coefficients) required to get acceptable SNR and how to ensure high data fidelity. This question is an optimization problem. The L_0 norm of the signal x ($\|x\|_0$) corresponds to the sparsity of the signal x. This is the number of non-zero elements in the vector. In terms of the computational process, the L_0 norm problem is not convex in nature, and it is difficult and impractical to solve the L_0 norm problem. The solution of the L_1 problem is the closest convex approximation to the solution of the L_0 norm problem. The L_1 norm provides the absolute sum of the elements of the vector. The L_1 norm penalizes the presence of a large number of coefficients. In other words, solving the L_1 norm problem corresponds to seeking the transform sparsity. As for the question of how to ensure data fidelity, the L_2 norm penalizes small errors less and large errors more significantly, by the quadratic nature of the norm. The L_2 norm is an iterative approximation process that accounts for data consistency.

The constrained optimization problem in reconstruction can be described by the following equation (Lustig et al. 2007):

$$minimize||\psi m||_1$$
$$s.t.||F_u \ m - y|||_2 < \varepsilon$$

where m is the desired image represented by a complex vector, y is the measured k-space data from MRI, ψ is the linear operator that transforms from pixel representation into a sparse representation and the threshold parameter ε is the parameter for error tolerance which controls the fidelity of the reconstruction to the measured data. To solve the problem, many strategies and algorithms (e.g., the non-linear conjugate gradient) have been studied and applied.

7.5.4 *Intuitive Example: Incoherence*

One of the most important requirements of CS in MRI is incoherence. Let us examine the importance of incoherence and the feasibility of CS in more detail. A simple 1D example with 480 data points of acquisition is shown in Fig. 7.10.

An example of undersampling patterns in the k-space is in Fig. 7.10b. Equispaced undersampling in the k-space results in coherent aliasing (Fig. 7.10c) and brings about an inherent ambiguity: it is impossible to distinguish between the original and shifted copies of a signal. Incoherent undersampling seems to incur random noise (Fig. 7.10d). The artifact that appears to be a noise is not "noise" per

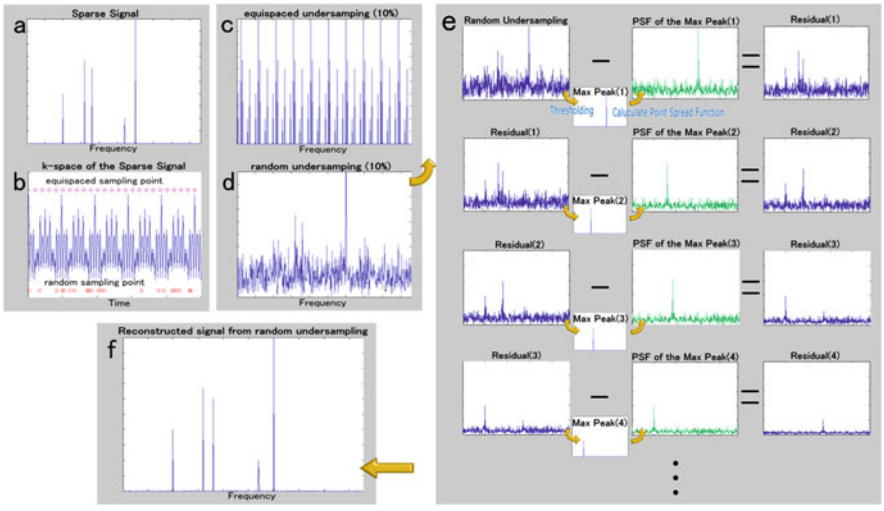

Fig. 7.10 Reconstruction from undersampled data. (**a**) Sparse signal. (**b**) Undersampling pattern in the k-space. The *circles* denote the sampling timings. (**c**) Equispaced undersampling results in coherent signal aliasing. (**d**) Pseudo-random undersampling results in incoherent aliasing. (**e**) Iterative reconstruction process from undersampled data. (**f**) Recovered signal by iterative reconstruction

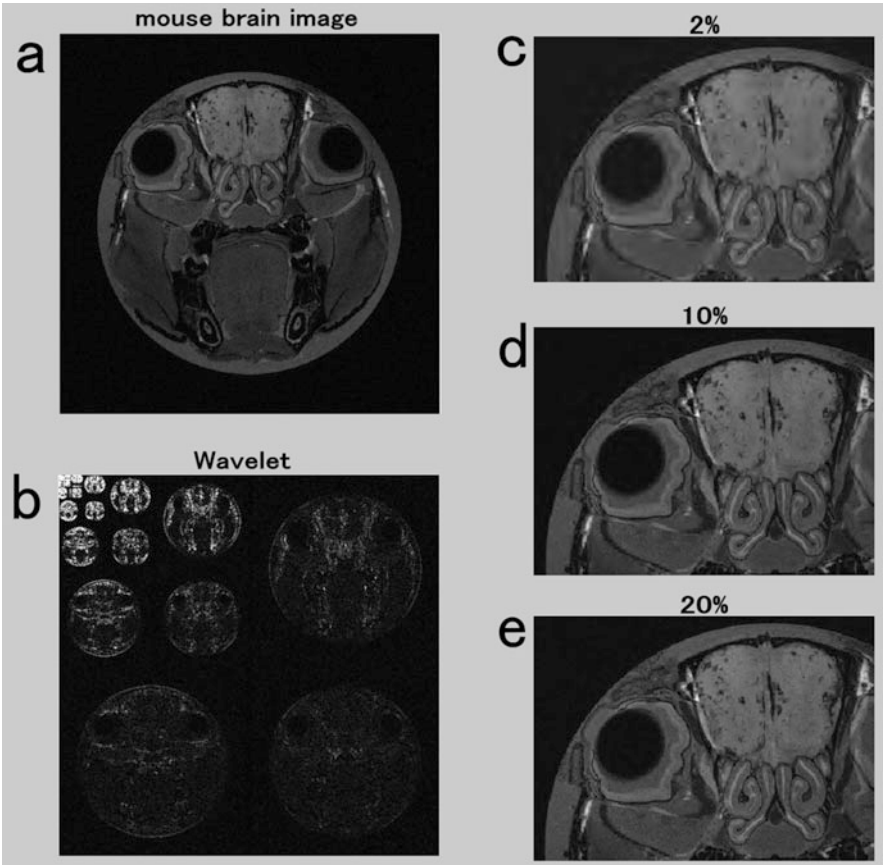

Fig. 7.11 Sparse approximation of a compressible image. The image is approximated by its largest wavelet coefficients. (**a**) Axial T1 mouse brain image. (**b**) Wavelet coefficients of the image. (**c–e**) Brain images are reconstructed from a subset of 2, 10, and 20 % of the largest coefficients

se but rather the energy spreading from each individual non-zero value of the original signal. Incoherent undersampling removes ambiguity in the original data (Fig. 7.10e, f). The pattern of Point Spread Function (PSF), a calculation of the spreading of the energy from the original signal, is dependent on the pattern of random sampling. If the random sampling pattern is not incoherent enough, the interference level increases and prevents accurate reconstruction.

In this example, the iteration procedure is repeated until all the significant signal components are recovered. The process corresponds to a sort of iterative algorithm for solving the optimization problem, and in effect performs threshold and interference cancellation at each iteration. Therefore, there is a close connection between this simple example of interference cancellation and formal and practical applications of CS in MRI.

The next example illustrates that sparse approximation can be available even with complicated images of the brain of the mouse (Fig. 7.11). Signal

approximation with 10 % of the largest coefficients results in good image quality. Nearly equivalent images can be gained using a significantly small number of coefficients. For CS in MRI to achieve the quality of image reconstruction that is shown in Fig. 7.11, it is necessary to develop a method to sample coefficients that correspond to those of the transform domain. In reality, it is not true that any sparse sampling pattern is possible; a practical sampling pattern is constrained by the hardware of MRI and physiological limitations.

7.5.5 Future of CS in MRI

The three requirements for the successful application of CS in MRI (as noted in 7.5.3) will be satisfied in many applications by ongoing developments. Potential applications of CS in MRI are based on some domain of sparsity: for example, sparsity in the temporal domain (e.g. dynamic imaging), sparsity in space (e.g. angiography), and sparsity as additive redundancy (e.g. resolution enhanced imaging). Even though different applications face different constraints, sampling trajectories and sparsifying transforms play key roles in matching the constraints. The ongoing development of CS in MRI, including the development of reconstruction algorithms, will bring new, fascinating applications and substantially benefit both the research and clinical usage of MRI.

7.6 Summary

In summary, MRI and MRS are proving to be extremely useful in neuroscientific research and neurological clinical practice. These powerful non-invasive tools are likely to continue to grow in importance in these fields and to gain ever more important clinical applications.

Exercises

1. What is nuclear magnetic moment?
2. What is resonance?
3. What is the resonance frequency of proton at 1.5 T?
4. What is the chemical shift?
5. What is the longitudinal relaxation time?
6. What is the transverse relaxation time?
7. What limits the resolution of MRI?
8. Why is the gradient coil necessary for MRI?
9. What is the contrast agent for MRI?

10. What factors influence water diffusion?
11. What is the Nyquist frequency?
12. What is the wavelet transformation?

References

Arnold, J.T., Dharmatti, S.S., Packard, M.E.: Chemical effects on nuclear induction signals from organic compounds. J. Chem. Phys. **19**, 507 (1951)

Bandettini, P.A.: Twenty years of functional MRI: the science and the stories. Neuroimage **62**, 575–588 (2012)

Basser, P.J., Mattiello, J., Le Bihan, D.: MR diffusion tensor spectroscopy and imaging. Biophys. J. **66**, 259–267 (1994)

Biswal, B., Yetkin, F.Z., Haughton, V.M., Hyde, J.S.: Functional connectivity in the motor cortex of resting human brain using echo-planar MRI. Magn. Reson. Med. **34**, 537–541 (1995)

Bloch, F., Hansen, W.W., Packard, M.: Nuclear induction. Phys. Rev. **69**, 127 (1946)

Brand, A., Richter-Landsberg, C., Leibfritz, D.: Multinuclear NMR studies on the energy metabolism of glial and neuronal cells. Dev. Neurosci. **15**, 289–298 (1993)

Candès, E.J., Romberg, J., Tao, T.: Robust uncertainty principles: exact signal reconstruction from highly incomplete frequency information. IEEE Trans. Inf. Theory **52**, 489–509 (2006)

Damadian, R.: Tumor detection by nuclear magnetic resonance. Science **171**, 1151–1153 (1971)

Donoho, D.L.: Compressed sensing. IEEE Trans. Inf. Theory **52**, 1289–1306 (2006)

Fox, M.D., Greicius, M.: Clinical applications of resting state functional connectivity. Front. Syst. Neurosci. **4**, 19 (2010)

Fox, M.D., Raichle, M.E.: Spontaneous fluctuations in brain activity observed with functional magnetic resonance imaging. Nat. Rev. Neurosci. **8**, 700–711 (2007)

Frahm, J., Krüger, G., Merboldt, K.D., Kleinschmidt, A.: Dynamic uncoupling and recoupling of perfusion and oxidative metabolism during focal brain activation in man. Magn. Reson. Med. **35**, 143–148 (1996)

Gill, S.S., Small, R.K., Thomas, D.G., Patel, P., Porteous, R., Van Bruggen, N., Gadian, D.G., Kauppinen, R.A., Williams, S.R.: Brain metabolites as ^{1}H NMR markers of neuronal and glial disorders. NMR Biomed. **2**, 196–200 (1989)

Goldstein, F.B.: The enzymatic synthesis of N-acetyl-L-aspartic acid by subcellular preparations of rat brain. J. Biol. Chem. **244**, 4257–4260 (1969)

Greene, J., Haidt, J.: How (and where) does moral judgment work? Trends Cogn. Sci. **6**, 517–523 (2002)

Haacke, E.M., Brown, R.F., Thompson, M., Venkatesan, R.: Magnetic Resonance Imaging: Physical Principles and Sequence Design. Wiley, New York (1999)

Hetherington, H.P., Mason, G.F., Pan, J.W., Ponder, S.L., Vaughan, J.T., Twieg, D.B., Pohost, G. M.: Evaluation of cerebral gray and white matter metabolite differences by spectroscopic imaging at 4.1 T. Magn. Reson. Med. **32**, 565–571 (1994)

Lauterbur, P.C.: Image formation by induced local interactions: examples employing nuclear magnetic resonance. Nature **242**, 190–191 (1973)

Le Bihan, D., Breton, E., Lallemand, D., Grenier, P., Cabanis, E., Laval-Jeantet, M.: MR imaging of intravoxel incoherent motions: application to diffusion and perfusion in neurologic disorders. Radiology **161**(2), 401–407 (1986)

Le Bihan, D., Urayama, S., Aso, T., Hanakawa, T., Fukuyama, H.: Direct and fast detection of neuronal activation in the human brain with diffusion MRI. Proc. Natl. Acad. Sci. U. S. A. **103**, 8263–8268 (2006)

Li, B.S., Wang, H., Gonen, O.: Metabolite ratios to assumed stable creatine level may confound the quantification of proton brain MR spectroscopy. Magn. Reson. Imaging **21**, 923–928 (2003)

Lustig, M., Donoho, D., Pauly, J.: Sparse mri: the application of compressed sensing for rapid mr imaging. Magn. Reson. Med. **58**, 1182–1195 (2007)
Magistretti, P.J., Pellerin, L.: Cellular mechanisms of brain energy metabolism and their relevance to functional brain imaging. Philos. Trans. R. Soc. Lond. B Biol. Sci. **354**, 1155–1163 (1999)
Moffett, J.R., Ross, B., Arun, P., Madhavarao, C.N., Namboodiri, A.M.: N-Acetylaspartate in the CNS: from neurodiagnostics to neurobiology. Prog. Neurobiol. **81**, 89–131 (2007)
Mori, S.: Introduction to Diffusion Tensor Imaging. Elsevier, Amsterdam/Boston (2007)
Mori, S., Barker, P.B.: Diffusion magnetic resonance imaging: its principle and applications. Anat. Rec. **257**, 102–109 (1999)
Mori, Y., Yoshioka, Y.: Visualization of immune cell dynamics in mouse brain with 11.7 T MRI. Proc. Intl. Soc. Magn. Reson. Med. **20**, 911 (2012)
Mori, Y., Umeda, M., Fukunaga, M., Ogasawara, K., Yoshioka, Y.: MR contrast in mouse lymph nodes with subcutaneous administration of iron oxide particles: size dependency. Magn. Reson. Med. Sci. **10**, 219–227 (2011)
Moseley, M.E., Cohen, Y., Mintorovitch, J.: Early detection of regional cerebral ischemic injury in cats: evaluation of diffusion and T2-weighted MRI and spectroscopy. Magn. Reson. Med. **14**, 330–346 (1990)
Ogawa, S., Sung, Y.W.: Functional magnetic resonance imaging. Scholarpedia **2**(10), 3105 (2007)
Ogawa, S., Lee, T.M., Kay, A.R., Tank, D.W.: Brain magnetic resonance imaging with contrast dependent on blood oxygenation. Proc. Natl. Acad. Sci. U. S. A. **87**, 9868–9872 (1990)
Pan, J.W., Twieg, D.B., Hetherington, H.P.: Quantitative spectroscopic imaging of the human brain. Magn. Reson. Med. **40**, 363–369 (1998)
Pauling, L., Coryell, C.D.: The magnetic properties and structure of hemoglobin, oxyhemoglobin and carbonmonoxy hemoglobin. Proc. Natl. Acad. Sci. U. S. A. **22**, 210–216 (1936)
Pouwels, P.J., Frahm, J.: Regional metabolite concentrations in human brain as determined by quantitative localized proton MRS. Magn. Reson. Med. **39**, 53–60 (1998)
Prichard, J., Rothman, D., Novotny, E., Petroff, O., Kuwabara, T., Avison, M., Howseman, A., Hanstock, C., Shulman, R.: Lactate rise detected by 1H NMR in human visual cortex during physiologic stimulation. Proc. Natl. Acad. Sci. U. S. A. **88**, 5829–5831 (1991)
Purcell, E.M., Torrey, H.C., Pound, R.V.: Resonance absorption by nuclear magnetic moments in a solid. Phys. Rev. **69**, 37–38 (1946)
Rabi, I.I., Zacharias, J.R., Millman, S., Kusch, P.: A new method of measuring magnetic moments. Phys. Rev. **53**, 318 (1938)
Ross, B.D., Blüml, S.: New aspects of brain physiology. NMR Biomed. **9**, 279–296 (1996)
Ross, B., Blüml, S.: Magnetic resonance spectroscopy of the human brain. Anat. Rec. **265**, 54–84 (2001)
Signoretti, S., Marmarou, A., Tavazzi, B., Lazzarino, G., Beaumont, A., Vagnozzi, R.: N-Acetylaspartate reduction as a measure of injury severity and mitochondrial dysfunction following diffuse traumatic brain injury. J. Neurotrauma **18**, 977–991 (2001)
Soares, D.P., Law, M.: Magnetic resonance spectroscopy of the brain: review of metabolites and clinical applications. Clin. Radiol. **64**, 12–21 (2009)
Srinivasan, R., Sailasuta, N., Hurd, R., Nelson, S., Pelletier, D.: Evidence of elevated glutamate in multiple sclerosis using magnetic resonance spectroscopy at 3 T. Brain **128**, 1016–1025 (2005)
Taylor, D.L., Davies, S.E., Obrenovitch, T.P., Doheny, M.H., Patsalos, P.N., Clark, J.B., Symon, L.: Investigation into the role of N-acetylaspartate in cerebral osmoregulation. J. Neurochem. **65**, 275–281 (1995)
Thulborn, K.R., Warterton, C.J., Matthews, P.M., Radda, G.K.: Oxygenation dependence of the transverse relaxation time of water protons in whole blood at high field. Biochim. Biophys. Acta **714**, 265–270 (1982)
Urenjak, J., Williams, S.R., Gadian, D.G., Noble, M.: Specific expression of N-acetylaspartate in neurons, oligodendrocyte-type-2 astrocyte progenitors, and immature oligodendrocytes in vitro. J. Neurochem. **59**, 55–61 (1992)

Wang, Y., Li, S.J.: Differentiation of metabolic concentrations between gray matter and white matter of human brain by in vivo ^{1}H magnetic resonance spectroscopy. Magn. Reson. Med. **39**, 28–33 (1998)

Zhang, X., Bearer, E.L., Perles-Barbacaru, A.T., Jacobs, R.E.: Increased anatomical detail by in vitro MR microscopy with a modified Golgi impregnation method. Magn. Reson. Med. **63**, 1391–1397 (2010)